

Seismic behavior of suspended building structures with semi-rigid connections

Yuxin Liu*¹ and Zhitao Lu²

¹*Civil Engineering Analysis, Candu Energy Inc. (CE), Mississauga, Canada, L5K 1B2*

²*School of Civil Engineering, Southeast University, Nanjing 210096, China*

(Received February 20 2014, Revised June 30, 2014, Accepted July 7, 2014)

Abstract. A method is presented in this paper to analyze the dynamic response behavior of suspended building structures. The effect of semi-rigid connections that link suspended floors with their supporting structure on structural performance is investigated. The connections, like the restrains in non-structural suspended components, are designed as semi-rigid to avoid pounding and as energy dissipation components to reduce structural response. Parametric study is conducted to assess the dynamic characteristics of suspended building structures with varying connection stiffness and suspended mass ratios. Modal analysis is applied to identify the two distinct sets of vibration modes, pendulum and bearing, of a suspended building structure. The cumulative modal mass is discussed to ensure the accuracy in applying the method of response spectrum analysis by SRSS or CQC modal combination. Case studies indicate that a suspended building having semi-rigid connections and proper suspended mass ratios can avoid local pounding failure and reduce seismic response.

Keywords: suspended building structure; semi-rigid connection; modal analysis; seismic response

1. Introduction

Some structural components such as floor slabs, ceilings, piping, and boilers are designed to hang on their supporting structures. For buildings, many suspended structures were built around the 1970s, including the Johannesburg Standard Bank Centre in South Africa, Munich landmark BMW Tower in Germany, Hong Kong HSBC Main Building, and Minneapolis Federal Reserve Bank in the United States. Some of them are described in the literature (Schueller 1977, Hart *et al.* 1985). Although many suspended buildings have been built around the world, there are no explicit specifications for suspended building structures in current design codes/standards against seismic loading. Conventional connections, such as rigid, are generally considered in design so that the available codes/standards can be applied.

On the other hand, design codes/standards do have specifications for non-structural suspended components, such as suspended ceilings and industry equipment. Past earthquakes show that suspended ceilings might experience severe damage during strong earthquake motions, such as the

*Corresponding author, Senior Civil Engineer, E-mail: yuxin.liu@candu.com, liuyuxine@yahoo.ca

damage of suspended ceiling and light fixtures in residential building during the Northridge earthquake (FEMA-74, 1994), and the damage in nuclear power plant during the Kashiwazaki-Kariwa earthquake (EPRI, 2008). The collapse of suspended ceilings might cause serious injuries, and even deaths of occupants and financial loss of properties. The failure is most likely caused by the lack of seismic restraints or poor design details on ceiling systems. To deal with ceiling failure due to strong earthquakes, building codes/standards (e.g., ASCE (2005), ASTM (2011)) require seismic restraints for suspended non-structural components based on quasi-dynamic analysis accounting for seismic loading. Seismic experience also indicated that when the suspended ceilings were adequately restrained per code provisions, the extent of such damage was reduced considerably (McKevitt, 1995). For suspended building structures, much work is required to attain the code/standard specifications for structural design purposes. Since restraints/connections are required for non-structural suspended components in current codes/standards, it is worth studying how the restraints, which connect suspended floors to their supporting structures, affect the response of suspended building structures.

From these building layouts, a suspended building can be defined as that having at least a floor hanging on the mega girder of core-tube or frame supporting structure. A suspended floor section has one or more storey floor slabs suspended on the same horizontal transfer girder. One of the problems in the suspended building structures is the structural instability due to up-shifted gravity loading in mega core-tube or frame supporting systems. Assessing the stability of suspended structures to ensure their robustness against all environmental loading is presented in another paper (Liu and Lu 2013). If the structural system is stable, there is still an issue with pounding between the suspended floors and their supporting structures as identified by Goodno and Gere (1976). This issue might cause local damage when the suspended portions impact on the supporting structure due to seismic loading. To resolve this pounding problem, deformable or semi-rigid connections can be designed in the suspended structural system to absorb energy. Damage of these connections is allowed and they can be replaced after a strong earthquake strike. This paper is to discuss the dynamic behavior of suspended building structures when semi-rigid connections are introduced. To this end, the structural modeling is presented first to account for the connections between suspended floors and their supporting structures. Then, the modal analysis method is used to investigate the dynamic characteristics, while the response spectrum method is utilized to predict the seismic response for structural design. Finally, case studies upon changing connection stiffness are performed to illustrate the seismic behavior of suspended building structures.

This paper is focused on discussing the modal nature of suspended building structures. Conventionally, the method of spectrum analysis has been applied during the design phase, as it generally leads to more conservative results than those obtained from time-history analysis. However, due to the special aspect of suspended structures having huge suspended mass/weight, spectrum analysis may not capture the actual seismic response of this type of structures. Thus, it is worthwhile in the future to further investigate the seismic behavior of suspended structures using the method of time-history analysis, where actually recorded or artificially generated time histories can be imposed onto structures. The results from response spectrum analysis will be compared with those from time history analysis, where the representative ground motions are compatible to the corresponding design spectra.

2. Modeling of suspended building structures

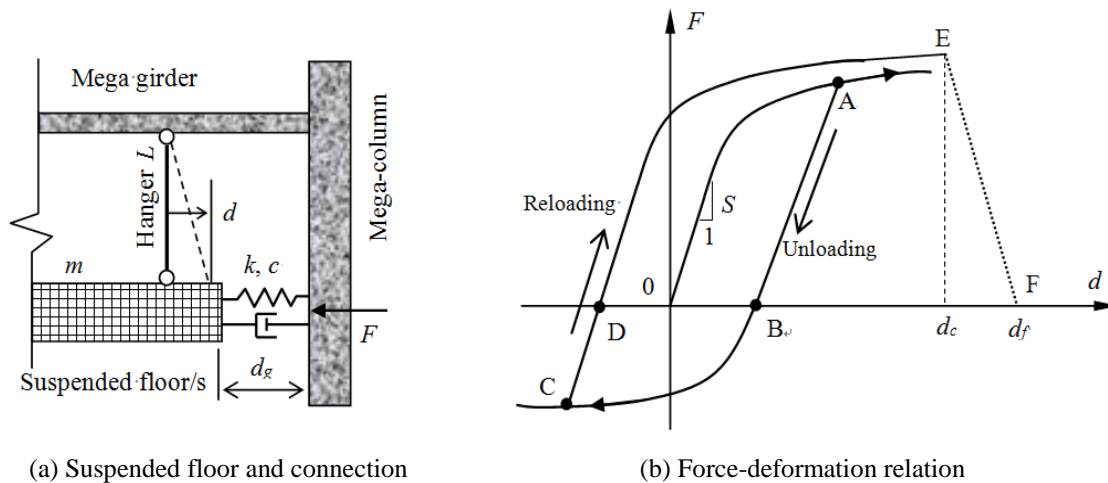
As in the conventional finite element analysis, the geometric and mechanical properties of a suspended building structure can be applied in the structural modeling. However, the geometrical stiffness due to suspended mass should be considered in the modeling. To simulate the effect of heavily suspended weight/mass on structural response, it is convenient to introduce a combined element model having lumped mass and connection stiffness for predicting and grasping the dynamic characteristics of suspended building structures. This section provides a way to develop the dynamic model for analyzing suspended building structures. The formulation of structural motion is derived to account for both connections and suspended mass.

2.1 Semi-rigid connections for suspended buildings

In order to model suspended building structures, this subsection presents a connection model to account for the effect of the suspended floor sections. As shown in Fig. 1(a), the suspended floor section of mass m is suspended on the transverse mega outrigger/girder with hanger of length L . When there is no connection between the suspended section and the mega supporting column/tube, a large sway of deflection d due to earthquake may cause pounding and localized damage. In practice, the suspended floor section should be connected somehow to the supporting structure to provide a horizontal access way for the occupants. Thus, the connection should be designed to take advantage of suspended-floor section in a controllable manner to degrade seismic vibration and avoid local pounding damage. To this end, the joint, which connects the vertical hanger to the transverse girder, should freely rotate to allow sway of the suspended section. How the stiffness k in Fig. 1(a) affects the swing of the suspended mass m may be found in the dynamic analysis of the suspended building systems (Liu and Lu 2013). Each horizontal joint, which connects a suspended floor to the supporting column/tube, should be designed as semi-rigid (Liu 2010) with stiffness k and damping coefficient c to transfer lateral loading and dissipate input energy. When the semi-rigid connections are determined to meet the three-level performances described below, suspended buildings can be designed as a type of structural control systems against seismic loading effectively.

The performance level corresponds to a normal operational state of the building that experiences minor seismic events. In this situation, the suspended building remains intact, and the connection between the suspended floor section and the supporting structure behaves elastically, i.e., the horizontal connection stiffness $k = S$ in Fig. 1(b). The force-deformation relationship shown in the figure represents the combined effect of the connected component and the damper. This combined connection is called as connection for short hereafter. It is seen that up to the first performance level, there is no structural damage to any building components, and the building is suitable for immediate occupancy after the earthquake event.

Second, the performance level requires protecting the occupants in the suspended building that experiences moderate earthquake events but local damage is intentionally allowed to dissipate earthquake energy. In this level, the horizontal semi-rigid connection in Fig. 1(a) has evolution of plasticity but there is no damage to the suspended floor, hanger, and supporting structure. The building can be re-occupied once the damaged semi-rigid connection, if any, is replaced to recover its function. Under moderate seismic loading, the horizontal connection experiences considerable stiffness degradation in dissipating input earthquake energy. Under transient seismic loading, the



(a) Suspended floor and connection

(b) Force-deformation relation

Fig. 1 Semi-rigid connection and response behavior

suspended building is enforced cyclically so that the force-deformation relationship of the connection follows the curve in Fig. 1(b). This cyclic model is for axial semi-rigid connections, and is similar to the model for flexural semi-rigid connections described in the literature (Liu 2010). It is seen that the connection is loaded in the positive direction following a monotonic nonlinear curve up to point A, and then unloading proceeds linearly to point B, at which the internal loading reduces to zero. This unloading may continue from point B following a nonlinear curve in the negative direction down to point C. From this point, linear reloading to point D occurs to indicate the completeness of the first loading cycle. Another new cycle will start from point D, and the cyclic loading is repeated until the end of the earthquake loading. Detailed information for determining the connection model and its parameters may be found in the previous research (Liu 2010). This model may not be exact, but recent research shows that the localized stiffness degradation affects the local response significantly but not the global response of the structure. Therefore, the hysteretic model described in Fig. 1(b) is considered sufficient to model the stiffness degradation of connections in suspended buildings.

Third, the performance level requires protecting the collapse of the suspended building that experiences major earthquake events, which are considered as a basis for design of suspended buildings. In this case, both stiffness degradation and strength deterioration occur as indicated in Fig. 1(b) from point E to point F with deflections d_c and d_f , respectively. It is assumed that the horizontal connection loses its function completely, and the suspended floor section is structurally separated from the vertical supporting structure. From Fig. 1(a) without the horizontal connection, the suspended floor section can swing freely. Such swing of the suspended-floor section further dissipates the earthquake energy to protect the supporting structure from collapse.

It is noted that when the connection is limited in the elastic range, the nonlinear connection behaviour can be ignored in the analysis. For further simplification, when the connection stiffness S in Fig. 1(b) is equal to zero, a configuration of suspended structures with free hung masses is achieved. Another extreme case is that when the connection stiffness S is infinite, a configuration of suspended structures with rigid connection is attained. Past experience from performance of suspension bridges and suspended roofs indicates that the influence of geometric

nonlinearity on these suspended structures may be significant due to large displacement. For suspended building structures to be studied, in addition to the material and/or connection nonlinearity as shown in Fig. 1, the effect of geometric nonlinearity on structural response should be taken into account. To capture such a nonlinear effect, step-by-step incremental analysis has to be carried out for the developed analysis models for suspended building structures. This paper is intended to establish a model for both static and dynamic analyses of suspended building structures. The following will discuss how the change in connection stiffness affects the structural response in the three specific levels presented above and the evolution of the whole nonlinear process is not covered hereinafter. Tracing the whole structural response accounting for both material and geometric nonlinearities will be considered in the future research.

2.2 Element analysis

To consider the effect of semi-rigid connections as discussed in the previous subsection on structural response, a beam-column element with end connection stiffness applied for framed structures (Liu *et al.* 2008, 2010) is employed in this study. This model can simulate the effects of semi-rigid connections, element-end damage, element inelasticity, element shear deformation, and geometrical nonlinearity on structural response. For dynamic analysis, the model is modified through adding lumped masses at its two ends as shown in Fig. 2(a), where L = element length, E = material Young's modulus, G = material shear modulus, I = cross-section moment of inertia, A = cross-section area, and A_s = equivalent shear area. Furthermore, terms r_j , t_j and n_j ($j = 1, 2$) are the corresponding bending, shearing and axial stiffness degradation factors, and unity is used for elastic analysis. Using these parameters, an element stiffness matrix can be derived and detailed expressions can be found in the literature (Liu 2009).

For a hanger with suspended floor mass, the model may be simplified from Fig. 2(a) to that in Fig. 2(b), where terms E , A , and L are respectively the Young's modulus, cross-section area, and length of the hanger. The upper end of the hanger has a rotational connection of stiffness R , which can be approximated to zero to conservatively ignore the rotational stiffness (Liu and Lu 2013). At low end 2, it is assumed that no axial restraint is imposed on the hanger, and the floor gravity load $P = m_s g$ is applied to account for the effect of gravitational force on stiffness. Meanwhile, the suspended floor mass m_s is connected to the mega vertical element with axial stiffness k_c and damping coefficient c_c . Stiffness k_c is similar to the rotational stiffness of semi-rigid connections. For this hanger model, only lateral stiffness is taken into account as geometrical stiffness. As discussed for a pinned hanger with suspended mass m_s , the hanger stiffness matrix is given by

$$[k]_s = S \begin{bmatrix} 1 & -1 \\ -1 & 1 \end{bmatrix} \quad (1)$$

in which S represents the stiffness from the suspended gravity load and end rotational restraints/connections. It is shown that the effect of the upper end rotational restraints on the lateral stiffness of hanger is insignificant (Liu and Lu 2013). Thus, when the upper end in Fig. 2(b) is assumed as a pin connection to ignore the rotational restraint, the lateral stiffness S becomes P/L , which will be used in the example analyses of this paper. The damping effect in the suspended hanger system may be simulated using the Rayleigh damping model. When the damping factor of c_s can be measured from testing, the damping matrix for the hanger can be directly expressed as

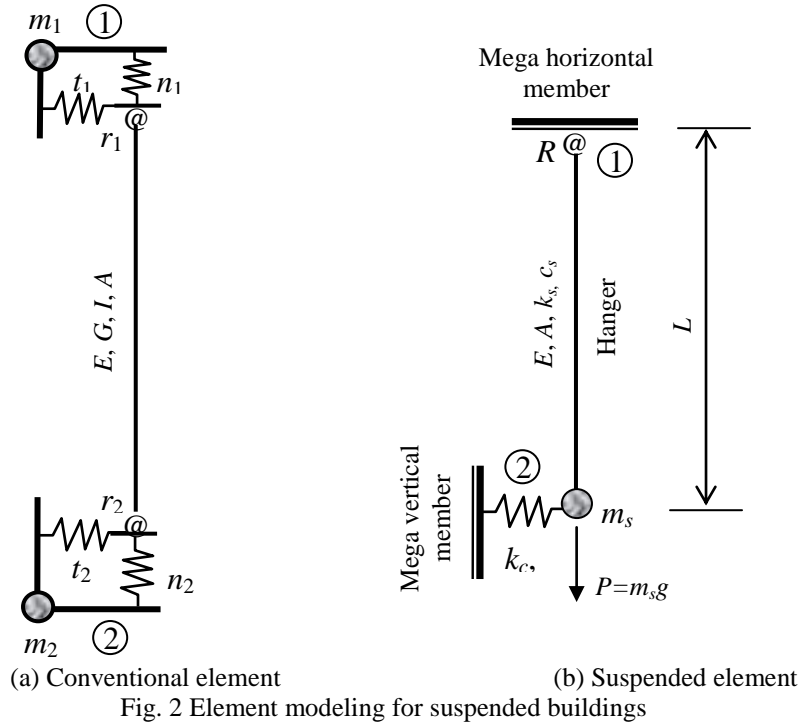


Fig. 2 Element modeling for suspended buildings

$$[c]_s = c_s \begin{bmatrix} 1 & -1 \\ -1 & 1 \end{bmatrix} \tag{2}$$

Note that c_s plays a role in damping the rotation of the hanger around the supporting point 1, to which a rotation damper may be attached to adjust the magnitude of c_s . Similarly, for the connection between the suspended floor/mass and the vertical supporting structure with stiffness k_c and damping coefficient c_c , the element stiffness and damping matrices can be expressed as

$$[k]_c = k_c \begin{bmatrix} 1 & -1 \\ -1 & 1 \end{bmatrix}; [c]_c = c_c \begin{bmatrix} 1 & -1 \\ -1 & 1 \end{bmatrix} \tag{3a, b}$$

which are similar to those matrices of a truss element in tension or compression. A translational spring and a damper may be designed to adjust the magnitude of coefficients k_c and c_c , respectively. Meanwhile, the distributed mass of the suspended floor section is assumed to be lumped to its mass centre, and a concentrated mass element m_s is added to node 2 in Fig. 2(b) for dynamic analysis.

2.3 Equations of structural motion

In the dynamic analysis of suspended structures, the aim is to compute the structural response, including displacements, accelerations, and internal forces (stresses) at certain positions of the structure as a function of time. Before conducting the dynamic analysis, a real structure needs to be mathematically idealised to some extent to obtain the element information as discussed in the

previous subsection. The continuous parameters of mass, damping and stiffness for the mega supporting element and suspended floor section are represented by element matrices. Integrating all the element mass matrices, element damping matrices, and element stiffness matrices by dynamic equilibrium, the equations of motion are obtained, which can be symbolically expressed as the following matrix equation

$$[M]\{\ddot{u}\} + [C]\{\dot{u}\} + [K]\{u\} = -[M]\{1\}\ddot{y}_0 \quad (4)$$

where $[M]$, $[C]$, and $[K]$ are respectively the mass, damping, and stiffness matrices for the structure with suspended floor sections discussed above. Vector $\{u\}$ represents the relative displacements of the structure to its base. Term $\{1\}$ is a vector whose every element is unity, and y_0 is the base motion due to earthquake. Note that Eq. (4) governs the motion just in one direction and it is often applied for symmetrical structures. After conducting the analysis in each direction, the combined response is obtained by the square root of sum of the squares (SRSS). However, when a building is not symmetric, the torsion effect should be taken into account, and Eq. (4) should be interpreted as a three-dimensional equation that accounts for the contributions from all three mutually perpendicular directions. In such a case, the three translational motions and, if required, the three rocking motions, should be enforced simultaneously to the base of superstructure.

Since the suspended-floor sections are linked to the supporting structure of a suspended building using semi-rigid connections, two steps can be taken to form the matrices in Eq. (4). In the first step, the supporting structure is modeled following the method in conventional dynamic analysis. For the supporting structure, there are no special requirements when assembling the mass matrix $[M]$ and stiffness matrix $[K]$, but some care should be given to forming the damping matrix $[C]$. For civil structures, the damping sources come primarily from internal friction within the material and the Coulomb friction at connections between components of a structure, whereas the damping effect due to the structure exposed to air is generally negligible. Thus, the resulting damping forces are a function of the strain (or deflections) in the structure. For an elastic structure, its damping force is proportional in magnitude to the internal elastic force, and at the connections, the damping force is almost constant, depending on the normal compressive force between the moving pieces. The structural damping force can be modeled using the hysteretic damping model. However, the equivalent viscous damping model is commonly employed because of its ease in mathematical treatment. To simplify the dynamic analysis, the damping matrix $[C]_1$ for the mega components (girder and core tube) of the supporting structure is assumed by using the Rayleigh damping model to linearly combine the corresponding mass and stiffness matrices of the supporting structure to get

$$[C]_1 = a_1[M]_1 + a_2[K]_1 \quad (5)$$

which maintains symmetry to facilitate the modal decomposition and transient analyses due to the symmetry of $[M]_1$ and $[K]_1$ for the supporting structure. In this model, the mass contribution is significant in the low frequency range, while the stiffness contribution is more significant in the high frequency range. The combination of Eq. (5) somehow averages the uneven variation with respect to frequency as discussed in determining the two coefficients a_1 and a_2 , which relates to the results of the modal analysis.

In the second step, the mass, stiffness, and the damping matrices in Eq. (4) are augmented to account for the suspended floors section by section. For an intuitive description, a shear-type

given by in which the correlated non-diagonal elements $-k_s$ and $-k_c$ are added. This procedure is repeated until all suspended-floor sections are assembled into the stiffness matrix $[K]$.

In augmenting the damping matrix $[C]$, the same procedure that formed Eq. (6) can be adopted and the location of element $c_s + c_c$ from Eqs. (2) and (3b) corresponds the augmented degree of freedom (DOF). The connection damping c_c of the suspended mass relates to only the bottom DOF that reflects the suspended floor being connected to the core tube. Thus, the combined damping value $c_b + c_c$ is obtained, where c_b comes from the first step relevant to the bottom-connection point. Meanwhile, the damping c_s of the suspended hanger relates to only the top DOF that reflects the suspended floor section being hung from the mega outrigger. Therefore, the combined damping value $c_t + c_s$ is integrated at the cross node of the mega outrigger and core tube, where c_t comes from the first step for the core tube relevant to the top-hanging point. This procedure is repeated until all suspended floor sections are assembled into the damping matrix $[C]$. Note that applying this procedure assumes that the element damping matrices of Eqs. (2) and (3b) can be determined, which in turn assumes that the properties of the rotational and translational dampers can be measured for the applied dampers. It is also noted that the total damping matrix $[C]$ formed by the previous two steps is symmetrical but may not have the same expression as the Rayleigh model in Eq. (5) for the supporting structure. When the damping coefficients in the second step are not available, the damping matrix may be estimated using the Rayleigh damping model as expressed in Eq. (5) once the total mass matrix $[M]$ and stiffness matrix $[K]$ are augmented. Because the damping matrix is symmetrical, the conventional method can be used in the modal decomposition.

3. Modal properties of suspended structures

Dynamic characteristics of suspended buildings can be interpreted using their modal properties. A mode of vibration is characterized by a modal frequency and its mode shape, and the modal properties are determined by solving a generalized mathematic eigen problem. A modal analysis is conducted to find the frequencies and the corresponding modes. These properties can be applied to assess the performance of building structures with pendulum floor sections. In addition, when the response spectrum method is utilized in the seismic analysis, the modal information is useful for selecting mode number and modes in the response spectrum analysis.

3.1 Modal characteristics of a simple example

In structural dynamics, the frequency and mode relate to the eigenvalue and eigenvector, which are concepts in the field of linear algebra. Eigenvalues and eigenvectors are the properties of a given matrix and all the eigenvectors span an eigenspace. In general, the eigen problem is defined in structural dynamics as the problem of free vibration without damping effect, causing the damping term and force term in Eq. (4) to vanish. Following this method, this subsection provides a discussion on the modal properties of a simple suspended system in Fig. 4, where the distributed mass of the supporting core tube is lumped as mass m_1 to its top. The core tube has lateral stiffness k_1 and damping coefficient c_1 . While for the suspended-floor section, the hanger has height L , lumped mass m_2 , and lateral stiffness k_2 . Following the procedure to integrate the stiffness and damping matrices, the first step is to form the mass matrix $[m] = m_1$ and the stiffness matrix $[K] = k_1$.

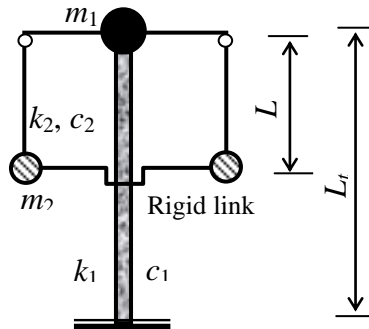


Fig. 4 An example model for optimal parametrical analysis

It is ready to generate the mass and stiffness matrices and expressed as

$$[M] = \begin{bmatrix} m_1 & 0 \\ 0 & m_2 \end{bmatrix}; \quad [K] = \begin{bmatrix} k_1 + k_2 & -k_2 \\ -k_2 & k_2 \end{bmatrix} \tag{7a, b}$$

in which the stiffness associated with the suspended floor section is k_2 , which is equal to m_2g/L in an extreme case (Liu and Lu, 2013). For the given parameters, the following relationships hold

$$\omega_s = \sqrt{\frac{k_1}{m_1}}; \quad c_s = 2\beta_s m_1 \omega_s = 2\beta_s \sqrt{m_1 k_1} \tag{8a, b}$$

where ω_s and β_s are the circular frequency and damping ratio for the supporting structure alone. For the portion hung on the supporting structure, the frequency and damping coefficients have the following relationships

$$\omega_h = \sqrt{\frac{k_2}{m_2}}; \quad c_h = 2\beta_h m_2 \omega_h \tag{9a, b}$$

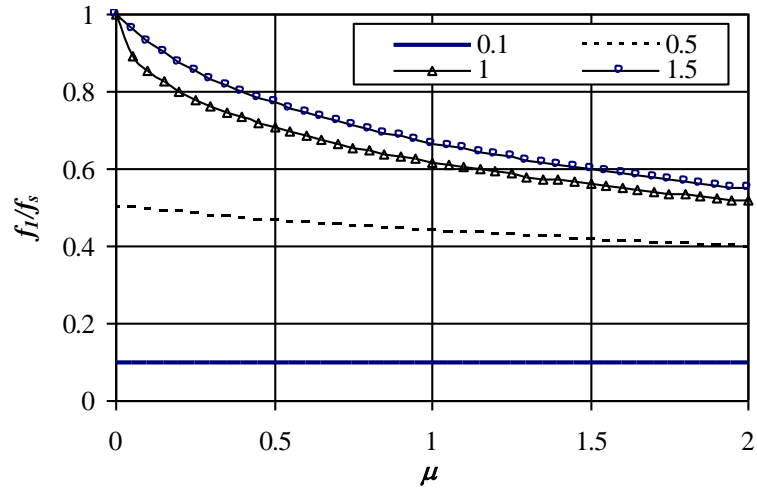
where ω_h and β_h are the circular frequency and damping ratio, respectively, for the hung-floor section alone. In order to investigate the effect of parameters on seismic response of the suspended structure, the following non-dimensional parameters are introduced

$$\mu = \frac{m_2}{m_1}; \quad \xi = \frac{\omega_h}{\omega_s} = \frac{f_h}{f_s}; \quad \eta = \frac{\omega}{\omega_s} = \frac{f}{f_s} \tag{10a, b, c}$$

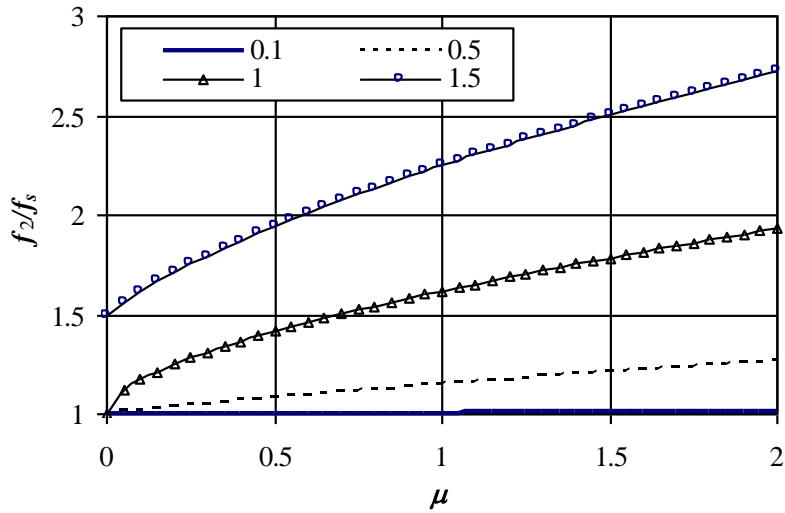
in which μ is the ratio of suspended mass to the lumped mass of supporting structure; ξ is the ratio of suspended frequency to the supporting frequency; and η is the ratio of the earthquake excitation frequency f to the frequency f_s of the supporting structure.

In order to find the frequency response of the suspended system, substituting Eq. (7) into the frequency equation Eq. (8) yields the eigenvalue equation. Solving the equation can find the two eigenvalues λ_1 and λ_2 , from which the corresponding two frequency ratios are given by

$$\eta^2 = 0.5 \left\{ 1 + (1 + \mu)\xi^2 \pm \sqrt{[1 + (1 + \mu)\xi^2]^2 - 4\xi^2} \right\} \tag{11}$$



(a) Response of frequency 1



(b) Response of frequency 2

Fig. 5 Frequency response with variation of frequency and mass ratios

which is related to the suspended mass ratio μ and frequency ratio ξ . To see the variation of the two frequency ratios, Eq. (11) is depicted in Fig. 5. It is seen that, when the mass ratio μ is considerably small and $\xi \leq 1$, the first two frequency ratios become $\eta_1 = \xi$ and $\eta_2 = 1$. This means that the first frequency f_1 tends to the pendulum frequency f_h and the second frequency f_2 tends to the supporting structural frequency f_s . In this special case, no interaction between the supporting

structure and the suspended mass occurs; i.e., the supporting structure and its suspended portion vibrate independently. With the increase of mass ratio μ , the first frequency ratio $\eta_1 (= f_1/f_s)$ is not greater than unity and decreases significantly when the frequency ratio ξ is larger as shown in Fig. 5 (a). On the other hand, the second frequency ratio $\eta_2 (= f_2/f_s)$ is not less than unity and increases significantly when the frequency ratio ξ is larger as shown in Fig. 5 (b) with the increase of mass ratio μ . From Eq. (11) and Fig. 5, when the frequency ratio ξ is quite small (say 0.1), the first frequency f_1 tends to the pendulum frequency f_h and the second frequency f_2 tends to the supporting structural frequency f_s . They nearly do not relate to mass ratio μ as shown in Fig. 5. Even though ξ reaches the value of 0.5, the two frequency ratios do not change significantly with the variation of mass ratio. When the frequency ratio ξ become larger (say 1), however, the first frequency ratio decreases but the second frequency ratio increases considerably. The first frequency ratio is sensitive to small value of ξ , while the second frequency ratio is sensitive to large value of ξ . These results indicate that increasing suspended mass ratio will decrease the frequency of suspended-floor section but increase the frequency of the supporting structure as the frequency of the supporting structure maintains constant. Adjusting the mass and frequency ratios can yield proper frequency distribution against dynamic loading.

In connection to the frequency nature above, the mode shape properties of the suspended system in Fig. 4 are discussed as follows. Upon substituting the obtained frequency in Eq. (11) into the eigenvector Eq. (7), the ratio of the displacement of supporting structures to the displacement of the suspended-floor section is given by

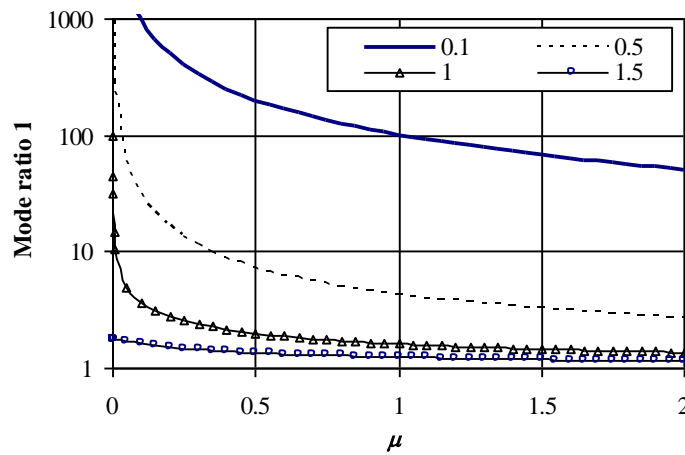
$$\frac{\phi_2}{\phi_1} = 1 + \frac{0.5}{\mu\xi^2} \left\{ - (1 - (1 + \mu)\xi^2) \pm \sqrt{1 - (1 + \mu)\xi^2 - 4\xi^2} \right\} \quad (12)$$

which describes two mode-displacement ratios, and their variations are depicted in Fig. 6 against the mass and frequency ratios. Corresponding to the first frequency, the displacement ratio of mode 1 from Eq. (12) is not less than unity with the increase of mass ratio ζ as shown in Fig. 6(a). This indicates that the supporting structure and the suspended-floor section move in the same direction. When the system has small suspended-mass ratio, the suspended mass has quite large displacement relative to the mass of the supporting structure. The suspended mass has a tendency to run away from the supporting structure. When the frequency ratio is small (say $\xi = 0.1$), the mode displacement ratio is considerably large, and compared to the suspended mass, the supporting structure remains nearly at rest. With the increase of frequency ratio ξ , such a relative displacement decreases. It is interesting to note from Fig. 6(a) that, for the conventional tuned mass damper (TMD) with suspended mass ratio up to 0.05 (Liu and Lu 2013), the difference of mode displacements may be remarkably large. For instance, this difference is over 100 when $\xi = 0.1$; and the difference is over 20 when $\xi = 0.5$. Thus, in design of a pendulum TMD, a larger frequency ratio should be applied to avoid pounding due to the excessive relative displacement. On the other hand, in design of suspended building, the suspended mass ratio is generally greater than 0.5, and the relative displacement can be controlled by adjusting the swing stiffness. In order to make use of the swing to dissipate energy, the stiffness of the suspended-floor section should

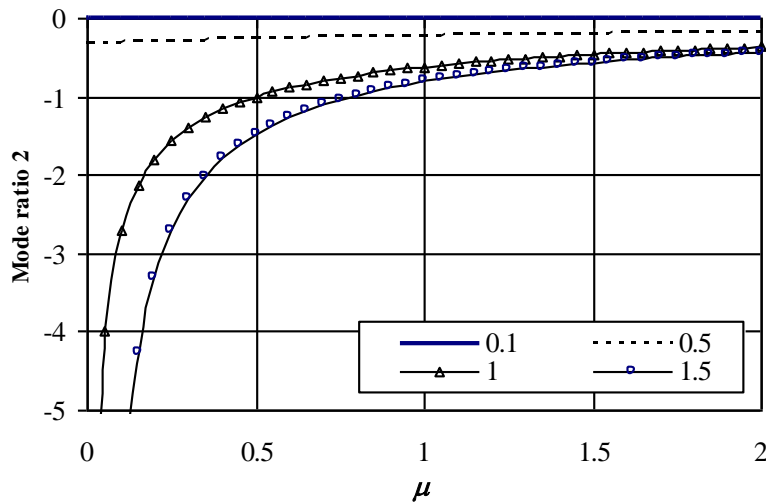
not be so big to lead to large frequency ratio and in turn to cause too small relative displacement.

Relevant to the second frequency, mode-displacement ratio 2 expressed in Eq. (12) with minus of the \pm symbol is not greater than zero with the increase of mass ratio μ and frequency ratio ξ as shown in Fig. 6(b). This indicates that the supporting structure and the suspended mass move in opposite direction. The suspended mass behaves in a tendency to pull the supporting structure back. When the frequency ratio is small (say ξ less than 0.5), the mode ratio has quite small absolute value and nearly has no change with the variation of mass ratio as shown in Fig. 6(b).

Particularly, for the conventional TMD with suspended mass ratio reached to 0.05 (Liu and Lu, 2013), the suspended mass nearly has no displacement compared to the mass center of the supporting structure when $\xi < 0.5$. With the increase of frequency ratio ξ (say 1), the second



(a) Response of mode shape



(b) Response of mode shape 2

Fig. 6 Mode shape factor with variation of frequency and mass ratios

mode-displacement ratio has large gradient and the suspended mass moves in the opposite direction with relative large displacement. For suspended building structure with mass ratio $\mu > 0.5$, the variation of the second mode ratio is not quite significant with the increase of the frequency ratio. This small relative displacement may be useful to reduce the pounding effect in the suspended system.

It is observed from the discussion above that suspended structures have different modal properties compared to the conventional bearing type of structures. The first frequency of the suspended system does not exceed the frequency of the supporting structure, while the second frequency is not less than the frequency of the supporting structure as shown in Fig. 6. In the first mode shape the two masses move in the same direction, and the displacement of the suspended mass is not less than the mass displacement of the supporting structure as shown in Fig. 6(a). However, in the second mode shape the two masses move in opposite direction as indicated in Fig. 6(b). A suspended portion sacrifices its stiffness to make the supporting structure gain stiffness so that the supporting structure may be protected against dynamic loading in general. The frequency and suspended mass ratios should be adjusted to achieve optimum structural response as expected.

4. Response spectrum analysis and effective mass

The modal properties discussed in the previous section alone may not be enough to be applied in assessing the response behaviour of suspended buildings. This section provides a discussion on the structural response of suspended buildings subjected to earthquake ground motions using the method of response spectrum analysis. This method is simple but conservative and has been extensively applied in seismic design since not all the modes are required for estimate of structural response. However, the effectiveness and accuracy of the modal superposition method need be reassessed when it is applied in analysis of suspended building structures because of different modal properties compared to conventional building structures.

4.1. Mode superposition method

On the basis of the modal analysis, the obtained modal properties can be applied in the dynamic analysis using the coordinate transformation $\{u\} = [\phi]\{v\}$, where $[\phi]$ is the mode matrix and $\{v\}$ is the generalized coordinate vector expanded in the modal space. The outstanding advantage of this method is that not all the modes are selected in the mode superposition analysis. In an extreme case for a conventional high-rise building, the first mode may be sufficient for predicting dynamic response. Without loss of generality, suppose N_m modes are used in the linear combination of eigenvectors to obtain the following expression

$$\{u\} = \sum_{i=1}^{N_m} v_i \{\phi\}_i = [\phi]\{v\} \quad (13)$$

Substituting Eq. (13) into the equations of motion in Eq. (4) and then multiplying the transpose of $[\phi]$ on both sides yields

$$[\underline{M}]\{\ddot{v}\} + [\underline{C}]\{\dot{v}\} + [\underline{K}]\{v\} = -[\phi]^T [M]\{1\}\ddot{y}_0 \quad (14)$$

where the $[\underline{M}]$ and $[\underline{K}]$ are symmetric matrices of generalized mass and stiffness in the modal

space with rank of N_m . When the Rayleigh damping model in Eq. (5) is applied, the generalized damping matrix $[C]$ in Eq. (14) is also symmetric. When the normality conditions in Eq. (9) are applied, the matrices $[M]$, $[C]$ and $[K]$ become diagonal so that Eq. (14) is decomposed into N_m independent equations

$$\ddot{v}_i + 2\beta_i\omega_i\dot{v}_i + \omega_i^2v_i = -\Gamma_i\ddot{y}_0 \quad (i = 1, 2, \dots, N_m) \quad (15)$$

in which β_i is the i th modal damping ratio and ω_i is the i th circular frequency of the system. In Eq. (15), term Γ_i is the i th modal participation factor having expression

$$\Gamma_i = \frac{\{\phi\}_i^T [M] \{1\}}{\{\phi\}_i^T [M] \{\phi\}_i} = \frac{\{\phi\}_i^T [M] \{1\}}{M_i} \quad (16)$$

where M_i is the i th generalized mass.

It is seen from the previous derivation that using the modal superposition method can decompose the n -DOF system into n or N_m -single DOF systems, and each single DOF system is subjected to ground motion y_0 . The responses v_i ($i = 1, 2, \dots, N_m$) of the N_m SDOF systems described in Eq. (15) can be solved separately and then the structural response is found using Eq. (13). Depending on the way specifying the ground earthquake input, there are two methods to find each DOF solution defined in Eq. (15). When the ground motion is defined by a time history, the direct-integration method is used to find the response. While the ground motion is defined by spectrum against frequency or period, the response spectrum method is applied to find the maximum response. Since the design earthquake is normally stipulated in design codes as acceleration response spectra versus period/frequency, the response spectrum method is commonly applied in structural design. Of course, once the time history compatible with the design response spectrum is determined, more accurate response can be predicted using the method of transient analysis. The following discussion focuses on the response spectrum method based on the design ground response spectrum.

After obtaining the maximum response R_i (e.g., the relative displacement, relative velocity and absolute acceleration, moment, shear or axial force) for mode i , the corresponding maximum structural response R is determined by combining all the modes of interest. In the modal superposition, the maximum structural response R can be obtained by use of the following general double sum combination (Wilson *et al.* 1981, NRC 2006)

$$R = \sqrt{\sum_{i=1}^m \sum_{j=1}^m R_i \rho_{ij} R_j} \quad (17)$$

where parameter ρ_{ij} is defined as a cross-modal coefficient that accounts for the correlation between modal responses. When the complete quadratic combination (CQC) method with constant modal damping is employed, the combination factor ρ_{ij} is determined by (Wilson *et al.* 1981)

$$\rho_{ij} = \frac{8\sqrt{\beta_i\beta_j}(\beta_i + \xi\beta_j)\xi^{1.5}}{(1 - \xi^2)^2 + 4\beta_i\beta_j(1 + \xi^2)\xi + 4(\beta_i^2 + \beta_j^2)\xi^2} \quad (18)$$

where the frequency ratio $\xi = f_j/f_i = T_i/T_j$, β_i and β_j are the i th and j th modal damping ratios used to evaluate the modal correlation. When parameter ξ approaches to unity, the modal correlation is relevant to the modal damping values alone, and only when $\beta_i = \beta_j$, complete correlation occurs with factor $\rho_{ii} = 1$. Thus, when two frequencies are close, the factor of Eq. (18) should be used in

the modal combination of Eq. (17). When ξ is small or quite large, the modal correlation is insignificant when the modal damping ratios are small; i.e., $\rho_{ij} \approx 0$ when $i \neq j$. Therefore, the following well-known expression of the Square Root of Sum of Squares (SRSS) method may be used as recommended in the design of nuclear power plants (CSA 2010)

$$R = \sqrt{\sum_{i=1}^{N_m} R_i^2} \quad (19)$$

According to the US NRC RG 1.92 (2006), the CQC method in Eq. (19) can be used provided that the following conditions are met: when $\beta \leq 2\%$ and $0.9 \leq \xi < 1$; or $\beta = 5\%$ and $0.8 \leq \xi < 1$; or $\beta = 10\%$ and $0.66 \leq \xi < 1$. When it is justified that there is no closely spaced frequencies to make sure ξ is quite small or large, the SRSS method can lead to sufficient accuracy of the combined response. Note also that when a three dimensional building structure is analysed respectively in the three mutual orthogonal directions, the total response can be obtained by combining the responses from all the perpendicular directions using the SRSS method.

In seismic design of building structures, the earthquake input to the superstructure is characterized by the specified design ground response spectra. When the ground spectral acceleration S_a is specified for a SDOF system with mass m , the earthquake impact force imposed on the mass is given by

$$F = mS_a = \frac{S_a}{g} mg = \alpha W \quad (20)$$

where W is the corresponding weight and $\alpha = S_a/g$ is a coefficient accounting for earthquake impact. Some design codes define the response spectrum of α as a function of the structural period T for seismic design. For instance, the Chinese code stipulates the following expression for seismic design of buildings (GB-500011 2010)

$$\frac{\alpha}{\alpha_{\max}} = \begin{cases} 0.45 + 10(\eta_2 - 0.45)T & T \leq 0.1 \\ \eta_2 & 0.1 < T \leq T_g \\ (T_g/T)^\gamma \eta_2 & T_g < T \leq 5T_g \\ 0.2^\gamma \eta_2 - \eta_1(T - 5T_g) & 5T_g < T \leq 6 \end{cases} \quad (21)$$

where α_{\max} is relevant to the design intensity and earthquake frequency specified for a site as given in Table 1. Term T_g is the site characteristic period given in Table 2 for different soil sites associated with different design groups. Parameters γ , η_1 and η_2 are relevant to the damping ratio β of the structure to be designed and the specific values are given in Table 3. Thus, the acceleration response spectrum is determined for seismic design and a typical shape of the spectrum is shown in Fig. 7 based on Eq. (21).

To apply Eqs. (20) and (21) in analyzing a multiple degrees of freedom (MDOF), the mode shape $\{\phi\}_i$ and period T_i of interest should be found first, and then the earthquake force is determined. For instance, if the i th mode is taken into account and the inertial force applied at the j th mass is given by

$$F_{ij} = \alpha_i \Gamma_i \phi_{ij} W_j \quad (22)$$

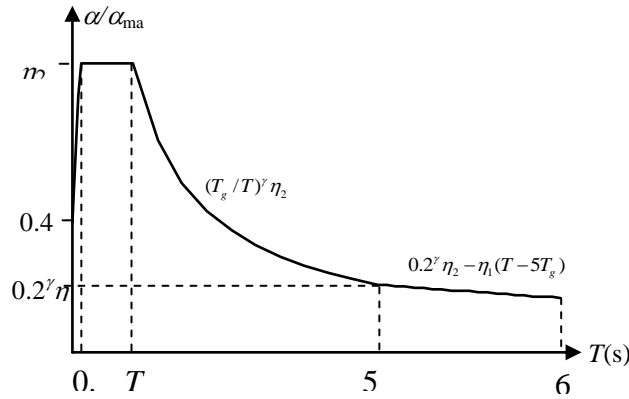


Fig. 7 Coefficient of ground response spectrum for seismic design

where α_i is the earthquake coefficient (g) for the i th mode and is determined from the α_{max} such as in Table 1, the characteristic period T_g in Table 2, and the coefficients in Table 3. The mode participation factor F_i is calculated using Eq. (16). In Eq. (22), term W_j is the weight corresponding to the j th mass.

For a suspended-floor mass, its seismic force determined using Eq. (22) is transmitted to the mega supporting girder and column according to the horizontal connection stiffness and the lateral stiffness of the suspended-floor section. Suppose the seismic force for a typical suspended-floor section in Fig. 3 is F_{is} for the i th mode from Eq. (22). The seismic force at the top hung point is F_{it} , and then the total seismic force, F_{it} , imposed on the mass of the mega girder in mode i is given by

$$F_{it} = F_{it} + \frac{k_s}{k_s + k_c} F_{is} \tag{23}$$

At the same time, if the seismic force on the bottom mass of the mega vertical column is F_{ib} , and then the total seismic force, F_{ib} , imposed on the mass of the mega-column mass in mode i is given by

$$F_{ib} = F_{ib} + \frac{k_c}{k_s + k_c} F_{is} \tag{24}$$

It is seen from Eqs. (23) and (24) that when the connection stiffness between the suspended-floor section and the vertical supporting column is zero, then the seismic force on the suspended mass is transmitted to the hung point when pounding does not occur. Once the seismic forces applied on the core tube or the mega vertical column are found, the inter-storey shear force in the j th storey of mode i is estimated by

$$V_{ij} = \sum_{q \geq j} F_{iq} \tag{25}$$

where the summation is conducted from storey j to the top storey. Based on the storey shear force of the vertical supporting structure in Eq. (25), the storey-drift response in mode i can be calculated by

$$\delta_{ij} = V_{ij} / k_j \tag{26}$$

Table 1 Maximum horizontal ground acceleration α_{\max} (g)

Design intensity	6	7	8	9
Frequent earthquake	0.04	0.08 (0.12)	0.16 (0.24)	0.32
Seldom earthquake	0.28	0.50 (0.72)	0.90 (1.20)	1.40

Note: values in brackets are applied to regions having design basis accelerations 0.15g and 0.3g

Table 2 Site characteristic period T_g (sec)

Design group	Site class				
	I ₀	I ₁	II	III	IV
1	0.20	0.25	0.35	0.45	0.65
2	0.25	0.30	0.40	0.55	0.75
3	0.30	0.35	0.45	0.65	0.90

Table 3 Earthquake spectrum coefficients versus damping ratios

β	γ	η_1	η_2
0.01	0.97	0.025	1.52
0.02	0.95	0.024	1.32
0.05	0.90	0.020	1.00
0.10	0.85	0.014	0.78
0.20	0.80	0.001	0.63
0.30	0.78	0.000	0.56

Meanwhile, the lateral displacement of the suspended-floor section is given by

$$\delta_{is} = \frac{F_{is}}{k_s + k_c} \quad (27)$$

When $k_c = 0$, the displacement from Eq. (27) represents that of the suspended mass relative to the mega hung girder; while $k_c = \infty$, this displacement reduces to that of the vertical column at the horizontal connection point. Note that a general computation can be achieved by incorporating into the static analysis method. To this end, substituting the mode inertial force from Eq. (22) of mode i into the structural stiffness equations to find the displacement vector, and then from element stiffness equation to find the internal forces for the corresponding mode.

The bending moments for each storey can be figured out once the storey shear forces are found from Eq. (25). When the modal response for each mode has been determined, the resultant response can be obtained by using Eq. (17) or (19). Using the CQC, especially the SRSS, combination method will overestimate the structural response because at a location the maximum responses for the modes under consideration may not occur at the same time. Thus, the response spectrum method based on CQC combination is conservative for design. If more accurate response is expected, modal time-history method can be applied in the analysis.

4.2 Cumulative modal mass

In some design codes, the cumulative modal mass is used as a criterion to assess the accuracy in the response spectrum analysis. In practice, not all the modes are required to consider in the modal

superposition since the modes with extreme high frequencies have little contribution to the structural response. The number of significant modes may be based the design code to cover the frequency ranging from 0 up to 33 Hz (CSA 2010), or to 50 Hz to account for the high frequency effect in seismic qualification by testing (IEEE-344 2005). Alternatively, the number of significant modes may be checked in such a way that the inclusion of any additional modes in the analysis does not increase the response by more than 10% (ASCE 4-98 2000). However, this may be difficult for engineers to apply because selecting the response (stress, strain, displacement, force, moment, or all of them) at which location is seems to be random. Even if this can be done, several rounds of reanalyses for complex structures are time consuming and may affect the construction schedule. Therefore, using the cumulative modal mass not less than 90% total mass to assess the accuracy may be more practical.

To derive the effective mass for suspended building structures, it is assumed that a static analysis is performed to apply the maximum inertial force due to ground earthquake motion as static loading. In this case, the stiffness equations can be expressed as

$$[K]\{u\} = \{F\} = -[M]\{1\}\ddot{y}_{0\max} \quad (28)$$

which is a special situation of Eq. (4) by ignoring the inertial and damping forces on its left-hand side and replacing ground acceleration time history by its maximum value. It is assumed that the modal properties are known from the modal analysis, and the unity vector $\{1\}$ in Eq. (28) is expanded in the modal space as

$$\{1\} \approx \sum_{i=1}^{N_m} c_i \{\phi\}_i \quad (29)$$

where N_m is the number of modes to be considered, and when all modes are taken into account, vector $\{1\}$ is exactly expanded in the modal space. Multiplying both sides of Eq. (29) by $\{\phi\}_i^T [M]$ yields the following expression

$$\{\phi\}_i^T [M] \{1\} \approx c_i \{\phi\}_i^T [M] \{\phi\}_i \quad (30)$$

where the modal normality condition in Eq. (9a) is applied. Compared with Eq. (16), it is found that the unknown combination factor c_i is equal to the modal participation factor; i.e.,

$$c_i \approx \Gamma_i \quad (31)$$

Substituting Eq. (31) into Eq. (29), and then into Eq. (28) yields the external force $\{F\}$ that is expanded in the modal space and the expression is given by

$$\{F\} \approx -[m] \sum_{i=1}^{N_m} \Gamma_i \{\phi\}_i \ddot{y}_{0\max} = -\sum_{i=1}^{N_m} \Gamma_i [m] \{\phi\}_i \ddot{y}_{0\max} \quad (32)$$

On the other hand, from equilibrium condition, the total base shear V of the superstructure is the summation of all the applied inertial forces above grade. Thus, from Eq. (28), the base shear V is expressed as

$$V = \{F\}^T \{1\} \approx -\sum_{i=1}^{N_m} \Gamma_i \{\phi\}_i^T [M] \{1\} \ddot{y}_{0\max} = \ddot{y}_{0\max} \sum_{i=1}^{N_m} M_i \Gamma_i^2 = \ddot{y}_{0\max} \sum_{i=1}^{N_m} M_{ei} = M_e \ddot{y}_{0\max} \quad (33)$$

where ρ_a is the cumulative modal mass ratio. It is seen from Eqs. (33) to (35) that when all modes are considered ($N_m = n$), the mass ratio $\rho_a = 1$, which means that all the mass of the superstructure is contributed to produce seismic force. To select sufficient number of modes in the response spectrum analysis, at least 90% ($\rho_a \geq 0.9$) of the actual mass is taken as a criterion to ensure the modal number for meeting the design requirement (ASCE 2006). From Eq. (35), the cumulative modal mass means how much of the total base shear is used in the seismic analysis.

It should be mentioned out that the ninety percent rule (of base shear) can ensure the accuracy for the response of conventional bearing type of building structures, but it may not guarantee the accuracy in some special situations. For instance, the missing mass effect should be taken into account for the dynamic analysis of nuclear piping systems (Neelwame 1993). As it will be shown in the following example analysis, the cumulative modal mass may not be a good indicator for the response accuracy of suspended building structures.

5. Example case studies

To illustrate the dynamic behaviour and seismic response of suspended structures, this section presents the analysis results for the model in Fig. 8, which is based on the core-tube type of suspended buildings (Liu 1999). In the first case analysis, the dynamic properties are discussed to show the variation of frequencies and mode shapes of the suspended structure. Then the nature of cumulative modal mass for the suspended structure is assessed to see the usefulness of the cumulative modal mass in the modal superposition method. Finally, seismic response spectrum analysis is performed to evaluate the contribution of modes, and comparison of seismic response is carried out to see the effectiveness of applying suspended-floor configuration to resist earthquake motion.

5.1. Modal characteristics

This example case study focuses on the modal analysis of the building structure in Fig. 7 to investigate the dynamic nature of a more general suspended building compared to that in Section 3. Assume that the height l for all storeys is 3.5 m, and the length L for all hangers is 3.5 m as well. A lumped mass m of 200 ton from each floor/roof and the adjacent storeys is concentrated at each elevation with transfer girder. At the elevation of the suspended floor level, a suspended mass m_s of 100 ton ($m/2$) is hung on the mega transfer girder, and another half of the mass m_c of 100 ton is concentrated at the core-tube supporting structure. For simplicity, the inter-storey stiffness k of 42000 kN/m is constant for all storeys. The damping coefficients c and c_c are not considered in the modal analysis. The influence of connection stiffness k_c between the suspended mass and the core tube on the modal properties is considered in two conditions: $k_c = 40000$ kN/m and $k_c = 0$. Then the frequency variation is assessed by changing the values of the connection stiffness and suspended mass ratios.

The stiffness matrix $[K]$ can be integrated following the procedure as explained for Eq. (6), and a diagonal mass matrix $[M]$ is ready to form based on the mass distribution shown in Fig. 8. To find the frequencies and modes, the FORTRAN code, developed based on the subspace iteration method (Liu 1999) and verified in predicting abnormal modes associated with zero/infinite frequencies in the large force method (Liu and Lu 2010), is applied in the analysis. Using the

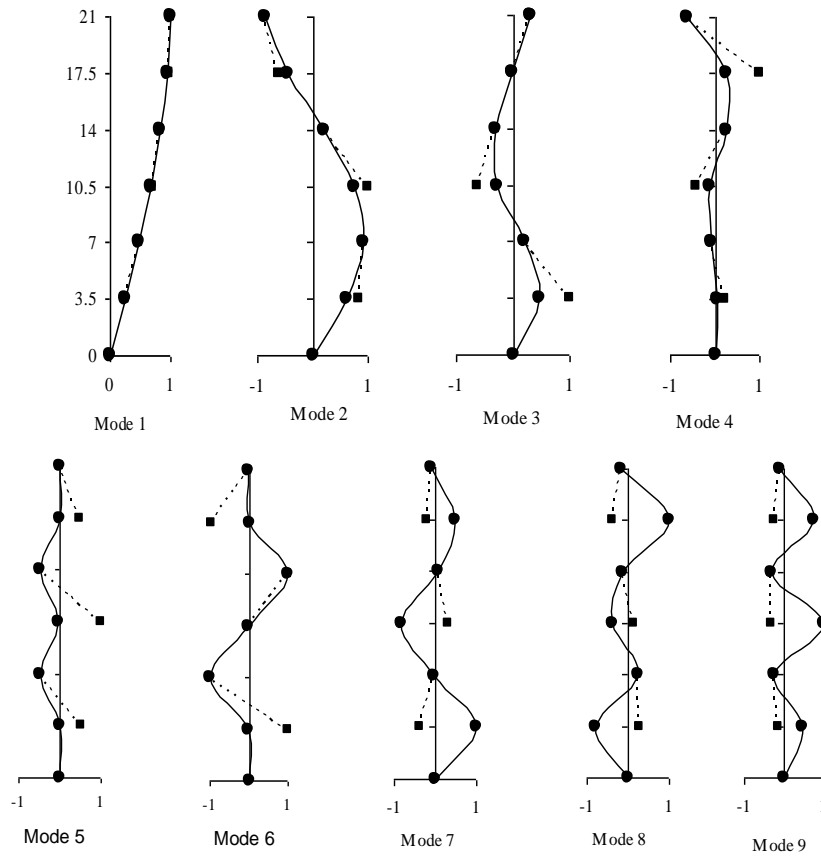


Fig. 9 Mode shapes with large connection stiffness ($k_c = 400\text{kN/m}$)

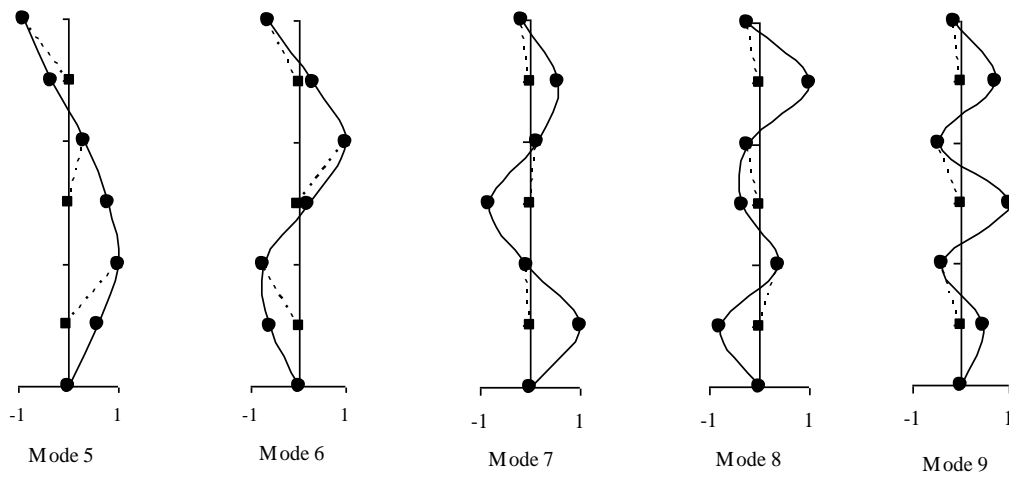


Fig. 10 Mode shapes without connection stiffness ($k_c = 0$)

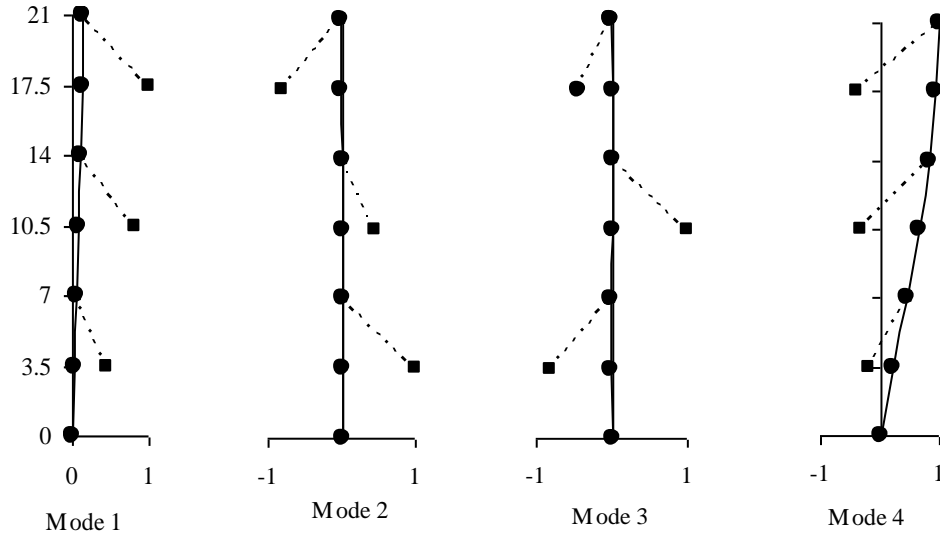


Fig. 10 Continued

Table 4 Influence of connection stiffness on frequencies (Hz)

k_c (kN/m)	Ratio %	f_1	f_2	f_3	f_4	f_5	f_6	f_7	f_8	f_9
∞	∞	0.556	1.637	2.618	3.448	4.082	4.484	—	—	—
40000	95.24	0.555	1.587	2.339	2.775	3.241	3.254	5.985	6.173	6.385
4000	9.52	0.535	0.980	1.015	1.200	1.912	2.841	4.803	5.213	5.579
400	0.95	0.377	0.412	0.414	0.688	1.835	2.821	4.707	5.142	5.520
40	0.1	0.273	0.284	0.284	0.653	1.829	2.819	4.698	5.138	5.513
4	0.01	0.258	0.267	0.268	0.650	1.829	2.819	4.697	5.135	5.513
0	0	0.256	0.265	0.266	0.650	1.828	2.819	4.697	5.135	5.513

Table 5 Influence of suspended mass on frequencies (Hz)

m_s (ton)	Ratio %	f_1	f_2	f_3	f_4	f_5	f_6	f_7	f_8	f_9
40	20	0.304	0.310	0.310	0.594	1.709	2.709	3.788	4.357	4.756
60	30	0.288	0.296	0.296	0.613	1.748	2.749	4.018	4.549	4.946
80	40	0.279	0.288	0.289	0.632	1.787	2.785	4.312	4.799	5.189
100	50	0.273	0.284	0.284	0.653	1.829	2.819	4.698	5.138	5.513
120	60	0.268	0.280	0.281	0.675	1.872	2.850	5.228	5.613	5.970
140	70	0.264	0.278	0.279	0.699	1.915	2.879	6.012	6.338	6.666
160	80	0.261	0.276	0.277	0.725	1.960	2.905	7.337	7.598	7.879

computer code for the first condition $k_c = 40000$ kN/m, the 9 modes of the structural system are illustrated in Fig. 9, where the small solid circles represent the masses lumped on the core tube and the small solid squares are the suspended-floor masses. It is seen for the suspended structure with large connection stiffness that the suspended masses move nearly together with the core-tube

masses at the corresponding elevations. With the increase of modes up to mode 6, the suspended masses separate from the corresponding connected masses and have larger and larger displacements. The separation generates strain energy in the connections and the large displacements of the suspended masses create kinetic energy to dissipate the earthquake input energy. For the last three modes in Fig. 9, the suspended masses and the masses at supports on the core tube nearly remain their original static state, but the corresponding masses on the core tube at the suspended-floor elevations have considerable deflections. Earthquake motion may not have the high energy to excite these high modes, as shown in the analysis of effective modal masses and the response spectrum analysis in the following two subsections.

In another extreme case with $k_c = 0$, the 9 modes of the structural system are depicted in Fig. 10. It is observed for the freely suspended floors that for the first three modes, the core-tube masses are nearly remained at rest, and the suspended floors have considerably large displacements. This means that earthquake motion with low frequency contents can easily excite the vibration modes of the freely suspended floors. In mode 4, the mode shape of the core tube is similar to the mode of a conventional building, and the suspended floors have small deflections and a tendency to pull the core tube back to its original static state. It is interesting to note that from mode 5 to 9 the suspended masses are nearly at rest, but the corresponding core-tube masses at the suspended-mass elevations have relative large deflections. This indicates that the suspended floors play a role in restoring the core tube to its original rest state.

The frequencies corresponding to the previous two case with $k_c = 40000$ kN/m and 0 are provided in Table 4. In addition, to consider the influence of connection stiffness on frequency, the calculated frequencies when $k_c = 4, 40, 4000, \text{ and } \infty$ kN/m are shown in the table. The second column shows the ratios of the connection stiffness to the core-tube storey stiffness (42000 kN/m) in percentile. In the extreme case when the connection stiffness approaches infinity, the conventional building construction is achieved and the six frequencies are given in Table 4. This table indicates that when the effect of suspended-floor construction is taken into account, the frequencies of the building change substantially. With the connection stiffness decreases from infinity, the first frequency f_1 gradually reduces to 0.256 Hz from 0.556 Hz. When the connection stiffness is close to the core-tube storey stiffness (95.24% of the core-tube stiffness) associated with the nine modes shown in Fig. 9, the first frequency f_1 changes only 0.18% but the higher frequencies have significant changes. For example, the 4th frequency f_4 of 2.775 Hz reduces 19.5% from 3.448 Hz. As the connection stiffness decreases to 400 kN/m (0.95% of the core-tube stiffness), the first frequency reduces 32%, while the 4th frequency f_4 of 0.688 Hz reduces 80% from 3.448 Hz. When the connection stiffness decreases to zero corresponding to the mode shapes shown in Fig. 10, the first frequency 0.256 Hz reduces 54% from 0.555 Hz and the 4th frequency f_4 of 0.65 reduces 81% from 2.755 Hz.

It is also noted that it may not be appropriate to compare the frequencies sequentially between a conventional structure and a suspended structure because the pendulum modes and bearing modes shown in Fig. 10 are distinct in the suspended structure. For instance, the first frequencies 0.556 Hz of the bearing-type structure cannot be compared with 0.256 Hz of the freely suspended structure. In fact, the modes 4 to 9 for the freely suspended structure are comparable to the six modes of the conventional structure. Thus, comparing f_4 to f_9 in the last row with f_1 to f_6 in the second row of Table 4, the corresponding frequency in the suspended structure increases; e.g., f_4 of 0.65 Hz increases 17% from the f_1 of 0.556 Hz in the second row. Because the total mass/weight is the same for the two systems, the increase of frequency may be equivalent to the stiffness increase of

the core-tube supporting structure due to the application of suspended construction. This may be one of the factors that suspended structures have good dynamic nature against transient loading.

It is observed from Table 4 that with small connection stiffness (say less than 1% of the core-tube storey stiffness), the first three frequencies decrease slightly with the reduction of the connection stiffness, and the rest 6 frequencies have insignificant change. For instance, for the first mode, frequency f_1 of 0.273 Hz with $k_c = 40$ kN/m is decreased 6.2% to 0.256 Hz with $k_c = 0$; after the third frequency, nearly no frequency change occurs. Thus, applying some connection stiffness between the suspended-floor sections and the core tube will not substantially change the suspended pendulum nature for structure control. Meanwhile, the small stiffness connection may be ignored in the dynamic analysis for simplicity.

To investigate the effect of suspended mass ratio on frequency, assume that mass $m_s + m_c = 200$ ton maintains constant and the horizontal connection stiffness $k_c = 40$ kN/m to keep the pendulum nature of the suspended floors and to avoid pounding. The suspended mass m_s is selected as values of 40 ton to 160 ton with increment of 20 ton. The computation results for the nine frequencies in each specified mass ratio are given in Table 5. It is seen that the frequency variation is divided into two groups. The first group includes the first three frequencies that correspond to the pendulum modes, while the second group includes the last six frequencies that correspond to the modes of the core-tube supporting structure. In the first group, with the increase of suspended mass ratio, the value of each frequency decreases. For instance, when the mass ratio is 20%, the first frequency f_1 is 0.304 Hz, which is 14% greater than 0.261 Hz when the mass ratio is 80%. In the second group, with the increase of suspended mass ratio, the value of each frequency increases. For instance, when the mass ratio is 20%, the fourth frequency f_4 is 0.594 Hz, which is 22% less than 0.725 Hz with 80% mass ratio. With the increase of mode number in the second group, the difference of the frequencies becomes more significant associated with the increase of suspended mass ratio. When the mass ratio is 20% the highest frequency f_9 is 4.756 Hz, which is 40% less than 7.879 Hz when the mass ratio is 80% of 200 ton. These results implicitly indicate that with the increase of suspended mass, the suspended-floor sections lose stiffness and the supporting structure gains stiffness.

5.2 Cumulative modal mass

To guarantee the accuracy in a response spectrum analysis, the effective mass participated in the mode superposition should not be less than ninety percent (ASCE 2006). As discussed in Section 4, the effective mass represents the portion of the total base shear that is taken in the seismic analysis. Since the base shear is commonly calculated at first and then distributed it to the superstructure for determining the structural displacements, internal forces and moments for structural design, the effective mass is naturally applied to estimate the number of modes that ensure accuracy of the base shear being applied. This example is to illustrate the application of the effective mass criterion to conventional and suspended building structures. The two cases corresponding to the modes in Figs. 9 and 10 are considered in the following.

In Case 1 with connection stiffness $k_c=40000$ kN/m, substituting each mode vector and mass matrix into Eq. (16) yields the modal participation factors of Γ_i , which are given in Table 6. Based on Eqs. (33) and (34), the modal effective mass M_{ei} and mass ratio ρ_i for mode i are found and given in the table. Finally, from Eq. (35) the cumulative modal mass ratio ρ_a with the variation of

Table 6 Comparison of effective masses and mass ratios

Mode (<i>i</i>)	1	2	3	4	5	6	7	8	9	
Case 1	Γ_i	1.249	0.409	0.427	0.037	-0.003	-0.004	0.132	-0.102	0.052
	M_{ei}	1045	109	39	0	0	0	4	2	1
	ρ_i	87.09	9.06	3.25	0.03	0.00	0.00	0.33	0.19	0.05
	ρ_a	87.09	96.16	99.41	99.43	99.43	99.43	99.76	99.95	100
Case 2	Γ_i	1.606	0.364	-0.137	1.025	0.383	-0.181	0.227	-0.142	0.064
	M_{ei}	503	24	3	566	72	14	11	5	1
	ρ_i	41.91	2.03	0.29	47.21	6.00	1.19	0.91	0.38	0.09
	ρ_a	41.91	43.95	44.23	91.44	97.44	98.62	99.54	99.92	100

modes is also provided in Table 6. It is observed from the table that since the connection stiffness is quite large and the structure is close to the conventional bearing type of structures, the first two modes alone have cumulative mass ratio 96.16%. This ratio is greater than the code required 90% of the total base shear force, and thus the rest modes can be neglected in the mode superposition analysis.

On the other hand, for Case 2 with connection stiffness $k_c = 0$, following the same computation procedure the values of Γ_i , M_{ei} , ρ_i , and ρ_a are found and shown in Table 6. It is seen that up to the fourth mode the cumulative mass ratio reaches 91.44%, which is greater than 90% of the total mass/base shear. However, using the 90% rule of mass participation for this suspended building structure may be inappropriate because some other significant modes are ignored. The modal mass ratio of mode 5 is 6%, which is considerably greater than 2.03% contribution from mode 2, and even the mass ratio 0.38% of mode 8 is greater than 0.29% contribution of mode 3. Thus, for this specific suspended building structure, the consecutively accumulated mass ratio may be inappropriate for judging the accuracy, and modes 1, 2, 4, 5 and 6 may be taken into account in the response spectrum analysis. These results show that the conventional cumulative mass ratio may not be a good indicator to show the accuracy in the response spectrum analysis of suspended building structures. In order to predict structural response much more accurate, the cumulative mass should be considered from the pendulum modes and the bearing modes. Alternatively, the transient time-history analysis with direct integration may be conducted to overcome such a difficulty in judging the accuracy. In the following subsection, the response spectrum analysis is performed to illustrate how each mode contributes to the whole structural response.

5.3 Results by response spectrum analysis

To show the mode contribution to the structural response, the suspended building system in Fig. 7 is applied again in the following analysis. For earthquake input motion, suppose the building is located at seismic design intensity 8, and the frequent earthquake event is taken into account. From Table 1 the maximum horizontal ground earthquake impact factor $\alpha_{\max} = 0.16$. In addition, the building is constructed on the soil site of class II associated with design group 2 so that the site characteristic period $T_g = 0.4$ sec from Table 2. As well, it is assumed that the structural damping ratio is 5%, which leads to $\gamma = 0.9$, $\eta_1 = 0.02$, and $\eta_2 = 1$ based on Table 3.

5.3.1 Comparison of SRSS and CQC methods

Assume the each suspended-floor mass $m_s = 100$ ton and $m_c = 100$ ton such that $\mu = 0.5$ as applied in the modal analysis in Subsection 5.1. When the connection stiffness k_c is assumed 40000 kN/m, the natural periods for the nine modes are 1.802, 0.631, 0.428, 0.362, 0.31, 0.308, 0.167, 0.162, 0.157 sec come from Table 4. Substituting the previous site parameters and these nine natural periods into Eq. (21) yields the corresponding nine α values 0.037, 0.082, 0.116, 0.135, 0.155, 0.156, 0.16, 0.16, 0.16. After the response for each mode is found, the SRSS method and CQC method with constant modal damping 5% are respectively applied to combine the modal responses. The maximum responses of displacement, acceleration for each node/mass, and shear force for each storey are provided in Table 7, where the relative difference δ is determined by $(\text{CQC}/\text{SRSS}-1)\times 100$. It is observed for this case with large connection stiffness that, using SRSS and CQC methods can get almost the same displacement response. The maximum difference of displacements is only 0.65%, and the maximum difference is 1.56% for the shear forces. Thus, from design point of view, using SRSS can yield accurate prediction of response. However, if acceleration response is expected for design of the mounted equipment (IEEE-344 2004), the CQC method should be applied since the SRSS method underestimates the acceleration by 17.08% at the first floor level but overestimates 9.34% at the fifth floor level.

For the purpose of comparison, suppose the connection stiffness k_c is changed into zero and other parameters in the previous case are remained unchanged. Based on the last row of Table 4, the corresponding natural periods for the nine modes are 3.902, 3.769, 3.761, 1.539, 0.547, 0.355, 0.213, 0.195, 0.181 sec. Similar calculation using Eq. (21) yields the nine earthquake impact α factors 0.03, 0.03, 0.03, 0.037, 0.093, 0.138, 0.16, 0.16, and 0.16. Once the response for each mode is found, the SRSS and CQC method with constant modal damping 5% are respectively used to combine the modal responses. The maximum responses of displacement, acceleration for each node/mass, and shear force for each storey are provided in Table 8. It is observed for this case with freely suspended floors that, using SRSS method can get displacement response of the supporting structure with maximum difference 1.78% relative to the CQC method, but for the suspended-floor masses the displacement difference is as high as 30.9% due to the closely spaced frequencies/periods. A 4.07% of maximum difference of the shear force occurs at the top of the core tube. Applying the SRSS and CQC methods will yield significant difference of acceleration responses for both the suspended floors and their supporting structure, and the maximum difference is 30.47%. Therefore, the CQC rather than the SRSS method should be applied in the mode superposition analysis of suspended structures with small connection stiffness.

Table 7 Structural response with large connection stiffness ($k_c = 40000$ kN/m)

Node/Storey		1	2	3	4	5	6	7	8	9
Displ. (mm)	SRSS	9.24	17.56	24.84	30.64	34.84	37.05	9.95	25.77	35.96
	CQC	9.27	17.59	24.85	30.64	34.83	37.03	10.01	25.78	35.95
	δ (%)	-0.38	-0.17	-0.04	0.00	0.03	0.05	-0.65	-0.04	0.03
Accel. (g)	SRSS	0.042	0.039	0.047	0.042	0.050	0.056	0.059	0.056	0.050
	CQC	0.050	0.040	0.043	0.041	0.046	0.055	0.062	0.055	0.049
	δ (%)	-17.08	-2.07	8.63	0.90	9.34	1.57	-3.80	2.09	1.49
Shear (kN)	SRSS	388	356.6	315.2	262.4	200.5	110.9	-	-	-
	CQC	389.5	356.7	315.1	261.8	199.1	109.2	-	-	-
	δ (%)	-0.39	-0.03	0.03	0.23	0.70	1.56	-	-	-

5.3.2 Assessment of mode contribution

For a conventional bearing-type building structure, three to six modes are generally taken in the response spectrum analysis to satisfy the 90% of cumulative modal mass. This may be different for suspended structures as discussed for the results in Table 8. To assess further the mode contribution to structural response, the displacement and acceleration at each node for each mode are analyzed in the following. Since a single mode consideration is considered without mode interaction, the following ratio is used as an indicator

$$r_{ik} = \frac{R_{ik}^2}{\sum_{j=1}^9 R_{jk}^2}, \quad i=1, \dots, 9; k=1, \dots, 9 \quad (39)$$

Table 8 Structural response without connection stiffness ($k_c = 0$)

Node/Storey		1	2	3	4	5	6	7	8	9
Displ. (mm)	SRSS	6.7	13.1	18.3	22.9	25.9	28.1	83.7	134.0	167.2
	CQC	6.9	13.3	18.4	23.0	25.9	28.1	120.0	134.5	142.7
	δ (%)	-1.78	-1.65	-0.87	-0.52	-0.23	0.04	-30.29	-0.37	17.17
Accel. (g)	SRSS	0.049	0.046	0.052	0.045	0.053	0.056	0.023	0.036	0.045
	CQC	0.059	0.047	0.049	0.045	0.046	0.055	0.033	0.036	0.038
	δ (%)	-16.46	-3.01	6.82	1.27	14.34	1.80	-30.47	-0.06	17.96
Shear (kN)	SRSS	283.0	269.4	227.7	207.3	148.5	115.1	-	-	-
	CQC	288.1	274.3	226.0	205.3	145.1	110.6	-	-	-
	δ (%)	-1.77	-1.79	0.75	0.97	2.34	4.07	-	-	-

Table 9 Contribution of each mode to structural response ($k_c = 40$ kN/m)

Node #		1	2	3	4	5	6	7	8	9
Mode # to displacement	1	19.2	19.9	20.3	20.9	20.8	21.2	75.5	96.8	96.4
	2	0.1	0.1	0.0	0.0	0.0	0.0	22.0	1.8	3.4
	3	0.0	0.0	0.0	0.0	0.0	0.0	2.4	1.3	0.2
	4	74.2	75.7	78.3	78.8	79.0	78.0	0.1	0.1	0.1
	5	5.6	4.2	1.3	0.2	0.1	0.7	0.0	0.0	0.0
	6	0.5	0.2	0.0	0.1	0.0	0.0	0.0	0.0	0.0
	7	0.4	0.0	0.0	0.0	0.0	0.0	0.0	0.0	0.0
	8	0.1	0.0	0.0	0.0	0.0	0.0	0.0	0.0	0.0
	9	0.0	0.0	0.0	0.0	0.0	0.0	0.0	0.0	0.0
Mode # to acceleration	1	0.0	0.1	0.2	0.5	0.5	0.5	70.0	92.1	91.8
	2	0.0	0.0	0.0	0.0	0.0	0.0	23.9	2.0	3.7
	3	0.0	0.0	0.0	0.0	0.0	0.0	2.6	1.4	0.2
	4	4.0	17.9	28.2	58.7	56.2	56.5	3.4	4.4	4.3
	5	18.6	61.2	29.6	6.7	5.4	32.9	0.1	0.0	0.0
	6	8.8	16.1	1.0	30.6	2.1	7.7	0.0	0.0	0.0
	7	54.0	0.3	34.9	1.2	14.8	1.3	0.0	0.0	0.0
	8	13.7	3.6	2.1	1.3	19.0	1.1	0.0	0.0	0.0
	9	0.9	0.8	3.9	1.1	2.0	0.1	0.0	0.0	0.0

where R_{ik} is the i th mode response at node k . The computation is conducted for the case where $m_s = 100$ ton and $k_c = 40$ kN/m, and the results are given in Table 9. This table shows that for displacement response, the first mode contribution to the deflections of the three suspended floors are 75.5%, 96.8%, and 96.8% but to the supporting structure only from 19.2% to 21.2%. The second and third modes mainly contribute to the deflection of the three suspended floors and have nearly no contribution to the supporting structure. For mode 4, the contribution to the displacement of the supporting structure from 74.2% to 78.0%, but only 0.1% to the suspended floors. Mode 5 still has some contribution to the supporting structure, but the contribution from the rest modes is negligibly small. This example shows that the first pendulum mode and the first bearing mode have strong interaction. Therefore, if 10% error is tolerable, the first two pendulum modes and the first two bearing modes may be selected in the response spectrum analysis for this specific case. For a general suspended building structure under a single-direction earthquake excitation, at least the first three modes corresponding to the suspended-floor sections and at least the first six modes corresponding to the supporting structure should be considered in the mode superposition method. Further research is needed to establish a reasonable criterion for the response spectrum analysis.

For mode contribution to acceleration, Table 9 indicates that the three pendulum modes play a main role for the suspended floors, and nearly no contribution to the supporting structure. The fourth mode contributes to the acceleration of the supporting structure from 4% to 58.7%, but only 3.4~4.4% to the suspended floors. These results show that for acceleration contribution, the interaction of the pendulum and bearing modes are insignificant. Unlike the mode contribution to displacement, the higher modes significantly have contribution to accelerations. For instance, mode 7 has 54% contribution to the acceleration of node 1, and mode 9 still has 3.9% contribution to the acceleration of node 3. Therefore, if node acceleration is required from the mode superposition analysis, the 90% rule of cumulative modal mass is not able to apply and more modes are needed for the mode combination.

5.3.3 Evaluate of seismic response reduction

The main advantage of suspended building construction is to create flexibility in arrangement of architectural space, but recently a research interest is given to design of suspended buildings as seismic control systems or seismic isolation system (Liu and Lu 2013; Mezzi and Parducci 2006). To see the seismic response reduction due to applying the suspended construction, this subsection provides a case study on the response of nodal displacements, nodal accelerations, and storey shear forces based on the response spectrum analysis. For the model in Fig. 8 with suspend mass $m_s = 100$ ton ($\mu = 0.5$), the response comparison is considered with varying the connection stiffness k_c from zero to infinity.

After performing a mode superposition analysis for each connection case, the nodal displacement response is listed in Table 10. These results show that the nodal displacements with $k_c = 40000$ kN/m are close to those of the conventional bearing-type structure ($k_c = \infty$). Thus, the displacement response with $k_c = 40000$ kN/m is taken as a reference to compute the difference δ relative to $k_c = 2000, 400, 40,$ and 0 kN/m. It can be seen from Table 10 that with the decrease of connection stiffness, the nodal displacements of the supporting structure reduce but the displacements of the suspended floors considerably increase. When $k_c = 2000$ kN/m, the nodal deflections of the supporting structure reduce from 6.8% to 7.3% (δ_1), but those of the three suspended floors increase from 64.8% to 116.8%. Particularly, for the case of freely suspended floors, the maximum top displacement is 28.1 mm, which reduces 24.2% from 37.3 mm; however, the maximum displacement of low suspended floor is 120 mm, which increases 1098.8% from

10.01 mm as indicated by the relative difference δ_4 . It is interesting to note that the nodal displacement reduction of the supporting structure with $k_c = 2000$ kN/m are in the same level of those with $k_c = 0$, but the sway deflections of the suspended floors are significantly reduced compared to the freely suspended case. Therefore, applying relative stronger connections/devices can still maintain the pendulum nature to reduce the displacements of the supporting structure. This also leads to the limitation of the excessive sway of the suspended-floor sections and avoids the pounding issue. Note that the occupants lived in the suspended-floor sections will feel large floor movement and may cause uncomfortable, but compared to injury even death due to strong earthquakes, such feeling of large displacement is tolerable.

Corresponding to the displacement response, the acceleration response is given in Table 11, where the response with $k_c = 40000$ kN/s is still taken as a reference to compare the difference relative to the selected other connection stiffness. It is seen from the table that with the decrease of connection stiffness, the nodal accelerations in low elevations of the supporting structure increase but the accelerations are considerably reduced for the suspended floors. For instance, when $k_c = 2000$ kN/m, the acceleration at node 1 of the supporting structure is 0.0581 g, which is 15.3% higher than 0.0504 g; while the acceleration at node 7 of the suspended floor is 0.0345 g, which is 44.7% lower than 0.0617 g when $k_c = 40000$ kN/m. Like the response of displacement, the change of accelerations is not so sensitive for small connection stiffness. Although the accelerations in the low elevations of the supporting structure are amplified due to the suspended floors, the accelerations in the low elevations of the suspended floors are reduced significantly. Thus, the combined effect makes the reduction of displacements of the supporting structure. It is interesting to note that the behaviour of acceleration reduction for the suspended floors has been observed in the experiments of bearing-mounted equipment and suspended-floor-mounted equipment (Marsantyo *et al.* 2000). This confirms the correctness of the method in this paper for the analysis of suspended building structures.

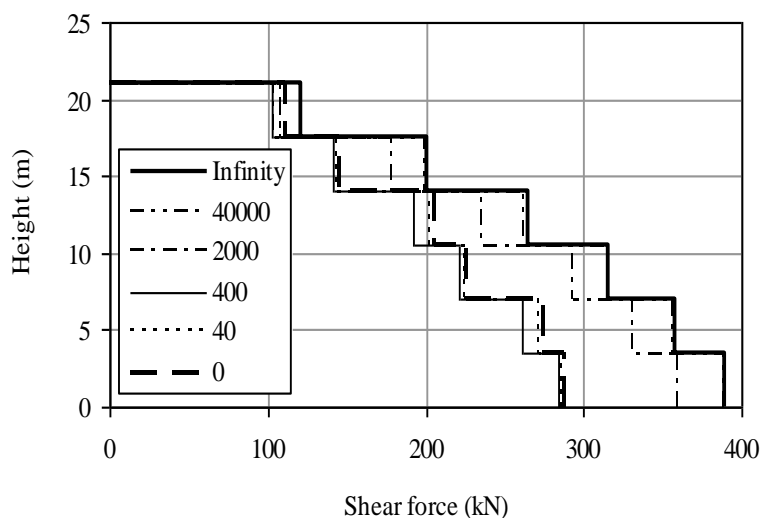


Fig. 11 Storey shear forces with various connection stiffness (k_c)

Table 10 Comparison of nodal displacements (mm)

Node #	1	2	3	4	5	6	7	8	9
$k_c = \infty$	9.27	17.66	24.90	30.73	34.91	37.14	-	-	-
40000 kN/m	9.27	17.59	24.85	30.64	34.83	37.03	10.01	25.78	35.95
2000 kN/m	8.58	16.37	23.16	28.52	32.40	34.34	21.70	43.28	59.24
400 kN/m	6.77	12.90	17.90	22.14	24.97	26.85	57.86	81.00	97.07
40 kN/m	6.83	13.22	18.29	22.80	25.68	27.79	108.30	124.00	133.30
0 kN/m	6.9	13.3	18.4	23.0	25.9	28.1	120.0	134.5	142.7
δ_1 (%)	-7.5	-6.9	-6.8	-6.9	-7.0	-7.3	116.8	67.9	64.8
δ_2 (%)	-27.0	-26.7	-28.0	-27.7	-28.3	-27.5	478.0	214.2	170.0
δ_3 (%)	-26.4	-24.8	-26.4	-25.6	-26.3	-25.0	981.9	381.0	270.8
δ_4 (%)	-26.0	-24.3	-25.8	-24.9	-25.6	-24.2	1098.8	421.7	296.9

Table 11 Comparison of nodal accelerations (g)

Node #	1	2	3	4	5	6	7	8	9
$k_c = \infty$	0.0486	0.0478	0.0485	0.0493	0.0500	0.0614	-	-	-
40000 kN/m	0.0504	0.0395	0.0432	0.0412	0.0458	0.0555	0.0617	0.0551	0.0491
2000 kN/m	0.0581	0.0454	0.0459	0.0418	0.0418	0.0506	0.0345	0.0482	0.0667
400 kN/m	0.0588	0.0463	0.0466	0.0416	0.0417	0.0515	0.0365	0.0485	0.0579
40 kN/m	0.0592	0.0473	0.0485	0.0445	0.0455	0.0550	0.0337	0.0379	0.0405
0 kN/m	0.0592	0.0475	0.0487	0.0449	0.0459	0.0554	0.0329	0.0362	0.0383
δ_1 (%)	15.3	14.9	6.2	1.3	-8.8	-8.8	-44.1	-12.5	35.9
δ_2 (%)	16.8	17.2	7.8	0.9	-9.0	-7.2	-40.9	-12.0	17.9
δ_3 (%)	17.5	19.8	12.1	8.0	-0.7	-0.8	-45.3	-31.2	-17.4
δ_4 (%)	17.5	20.1	12.7	8.9	0.3	-0.1	-46.7	-34.3	-22.1

Table 12 Comparison of storey shear forces (%)

Storey #	1	2	3	4	5	6
40000 kN/m	0.00	-0.31	-0.28	-0.87	-0.99	-9.30
2000 kN/m	-7.50	-7.29	-7.09	-10.72	-11.29	-13.79
400 kN/m	-27.01	-26.97	-29.91	-27.04	-29.44	-14.78
40 kN/m	-26.39	-24.12	-29.02	-23.17	-28.34	-9.22
0 kN/m	-26.03	-23.34	-28.48	-22.26	-27.85	-8.14

For linear analysis of elastic structures, the internal forces are proportional to the relative nodal displacements so that for this example the storey shear forces have almost the same nature of the nodal displacements. Because the flexible connections between the suspended floors and their supporting structure, the internal forces in the suspended portions are generally small. Thus, the shear forces of the supporting structure shown in Fig. 11 are compared in the following. It is observed that the two cases of large and infinite connection stiffness have almost the same distribution of shear forces. The shear force reduction is more significant in the low elevations than the upper elevations. With quite large connection stiffness (say, $k_c = 2000$ kN/s), the storey shear forces are reduced to some extent. When the connection stiffness is not greater than 400

kN/m, the difference of reduction is not so great. Taking the shear response with infinite connection stiffness of k_c as the reference, the corresponding relative differences of shear forces are summarized in Table 12 to show numerically the efficiency of shear reduction. It can be seen that with the decrease of connection stiffness, the shear forces below storey 6 of the supporting structure decrease significantly. For instance, when $k_c = 400$ kN/m, the force in storey 1 is 284.3 kN, which is 27.01% lower than 389.5 kN when $k_c = \infty$; while the force in storey 6 is 102.6 kN, which is only 14.78% lower than 120.4 kN. In general, with flexible connection, the storey shear forces of this suspended building structure are reduced in comparison with the conventional bearing type structure, and the maximum reduction is around 30%. Therefore, designing buildings with suspended floors can generate earthquake control systems to reduce seismic response of the supporting structures although the suspended-floor sections may have large sway.

6. Summary and conclusions

Presented above include the development of dynamic model and analysis results for suspended building structures. The dynamic equations are established based on the pendulum concept presented in the previous study (Liu and Lu 2013). In light of the dynamic model, both modal and response spectrum analyses are carried out to investigate the dynamic behaviour of suspended building systems. The cumulative modal mass is discussed on the application of the response spectrum method to the seismic design of suspended structures. Based on this study, the following conclusions can be drawn regarding the structural nature and dynamic performance of suspended building structures.

When the pendulum nature and semi-rigid connections are considered in the building structure, the resulting structural system becomes a passive control system. Three steps are taken to establish the dynamic model for the seismic analysis. First, the mega supporting structure, including the vertical tubes and transverse girders, is modeled as a conventional structure, whose mass and stiffness matrices are assembled using the direct stiffness method, from which a damping matrix is formed using the Rayleigh model. Second, each suspended floor section is modeled as a pendulum system, where the lateral stiffness due to suspended weight is taken into account. Third, each connection between the supporting structure and the suspended floors is modeled as a semi-rigid connection with material damping. In the dynamic analysis, the mass, damping, and stiffness matrices obtained in step 1 for the supporting structure are augmented by adding the element matrices of each suspended-floor section from step 2 and the corresponding connection from step 3.

Results of modal analysis show that the modes of a suspended building structure are distinctly divided into two groups. In the first group, each mode is referred to as a pendulum mode corresponding to the suspended-floor sections; while each mode in group two is called a bearing mode related to the supporting structure. Upon adjusting the suspended mass ratio and connection or tie stiffness, the modal properties change considerably. This leads to a possibility to design suspended building structures as effective control systems against seismic loading.

Based on the results of response spectrum analysis, care should be given to the selection of the number of modes from the two distinct pendulum and bearing groups. For conventional bearing-type building structures, sequential modes starting from the first mode are commonly selected in the mode superposition analysis. However, for a suspended building structure, the modes should

be selected from the first several pendulum and bearing modes for the analysis. The CQC rather than the SRSS method should be applied to combine the mode contributions of suspended building structures. When acceleration response is expected, more modes should be selected to ensure the accuracy of predicted results. Seismic response spectrum analysis reveals that designing buildings with suspended floors can reduce the displacements and storey shear forces of the supporting structures compared to the conventional bearing type of structures. Although the displacements of the suspended floors are increased with the decrease of connection stiffness, the large uncomfortable sway is tolerable for occupants compared to injury or death. In general, suspended buildings can be designed as effective structural systems to mitigate seismic response and protect occupants from strong earthquake motions.

Due to the distinct pendulum and bearing modes, the method of response spectrum analysis may not completely capture the vibrational behaviour of suspended building structures. Meanwhile, the maximum responses from the selected modes generally do not occur at the same time. Note that complex eigenvalue analysis is of interest in the future to investigate the damping effect on the suspended structures. The method of transient time-history analysis will be performed to validate the analytical results from the spectrum analysis. Further research is needed to assess the established model of suspended building structures from the viewpoint of structural control.

It should be pointed out that the above conclusions are drawn based on enforcing horizontal earthquake motions to the structures alone. Because the first several modes in horizontal direction might dominate the horizontal seismic response, the contribution of vertical modes to the horizontal response may not be significant. Thus, accounting for the interaction of horizontal and vertical ground motions may not considerably change the horizontal response and in turn the conclusions from this study. However, further research is needed to study the structural response to take such an interaction into account.

Acknowledgment

This work was funded partially by the grants (No. 59338130, 59508010, and 59978008) from the National Natural Science Foundation of China, and great appreciation is acknowledged for such financial supports.

References

- ASCE 4-98 (2000), *Seismic Analysis of Safety Related Nuclear Structures and Commentary*, American Society of Civil Engineers, Reston, Virginia, USA.
- ASCE 7-05 (2006), *Minimum Design Loads for Buildings and Other Structures*, American Society of Civil Engineers, Reston, Virginia, USA.
- ASTM (2011), E580/E580M-11be1, Standard Practice for Installation of Ceiling Suspension Systems for Acoustical Tile and Lay-in Panels in Areas Subject to Earthquake Ground Motions, Developed by Subcommittee: E33.04, ASTM International.
- CSA N289.3-10 (2010), *Seismic Design and Qualification of Nuclear Power Plants*, Canadian Standard Association, Mississauga, Ontario, Canada.
- EPRI (2008), 1016317, EPRI independent peer review of the TEPCO seismic walkdown and evaluation of the Kashiwazaki-Kariwa nuclear power plants: A study in response to the July 16, 2007, NCO earthquake.

- Electric Power Research Institute (EPRI), Palo Alto (CA, USA).
- FEMA-74 (1994), Reducing the risks of nonstructural earthquake damage. Federal Emergency Management Agency, Washington, DC (USA).
- GB-50011 (2010), *Code for seismic design of buildings*, China Architecture and Building Press, Beijing, China.
- Goodno, B.J. and Gere, J.M. (1976), "Earthquake behaviour of suspended-floor buildings", *J. Struct. Div. (ASCE)*, **102**(5), 973-992.
- Hart, F., Henn, W.H. and Sontag, H. (1985), *Multi-Storey Building in Steel*, 2nd Edition, Great Britain at the University Press, Cambridge, UK.
- IEEE 334 (2005), *IEEE Recommended Practice for Seismic Qualification of Class 1E Equipment for Nuclear Power Generating Stations*, The Institute of Electrical and Electronics Engineers, Inc., New York, NY, USA.
- Liu, Y. (1999), "Optimum Parameter Analysis and Earthquake-evadable Study on Core-Tube Suspension Building Structure Control Systems," *Ph.D. Thesis*, School of Civil Engineering, Southeast University, China.
- Liu, Y. (2009), "Hybrid member stiffness matrix accounting for geometrical nonlinearity and member inelasticity in semi-rigid frameworks", *Eng. Struct.*, **31**(12), 2880-2895.
- Liu, Y. and Lu, Z. (2010), "Methods of enforcing earthquake base motions in seismic analysis of structures", *Eng. Struct.*, **32**(8), 2019-2033.
- Liu, Y. (2010), "Semi-rigid connection modeling for steel frameworks", *Struct. Eng.Mech.*, **35**(4), 431-457.
- Liu, Y. and Lu, Z. (2013), "Seismic performance and storey-based stability of suspended building structures", *Adv. Struct. Eng.*, accepted.
- McKevitt, W.E., Timler, P.A.M. and Lo, K.K. (1995), "Nonstructural damage from the Northridge earthquake", *Can. J. Civil Eng.*, **22**(2), 428-437.
- Marsantyo, R., Shimazu, T. and Araki, H. (2000), "Dynamic response of non-structural systems mounted on floors of buildings", *Proceeding of the 12th World Conference on Earthquake Engineering*, Auckland, New Zealand.
- Mezzi, M. and Pardini, A. (2006), "Conceptual seismic design and state-of-the-art protection systems," in *The 8th U.S. National Conference on Earthquake Engineering*, San Francisco, CA, USA.
- Neelwame, N. (1993), "Convergence in response spectrum analysis, global versus local modes", *Proceeding of the 12th International Conference on Structural Mechanics in Reactor Technology*, Stuttgart, Germany.
- NRC RG1.92 (2006), "Combination modal responses and spatial components in seismic response analysis", Revision 2, Nuclear Regulatory Commission, Washington, DC, USA.
- Schueller, W. (1977), *High-Rise Building Structures*, John Wiley & Sons, New York, NY, USA.
- Wilson, E.L., Der Kiureghian, A. and Bayo, E.P. (1981), "A replacement for the SRSS method in seismic analysis", *Earthq. Eng. Struct. Dyn.*, **9**(2), 187-192.